Optical Spectra and Band Structure of AgxGaxGe1-xSe2 (x=0.333, 0.250, 0.200, 0.167) Single Crystals: Experiment and Theory

ARTICLE *in* THE JOURNAL OF PHYSICAL CHEMISTRY B · NOVEMBER 2013

Impact Factor: 3.3 · DOI: 10.1021/jp410786w · Source: PubMed

6 AUTHORS, INCLUDING:

Ali H Reshak
University of West Bohemia
477 PUBLICATIONS **3,415** CITATIONS
SEE PROFILE

O. V. Parasyuk
Lesya Ukrainka Eastern European National Un…
281 PUBLICATIONS **1,488** CITATIONS
SEE PROFILE

H. Kamarudin
Universiti Malaysia Perlis
365 PUBLICATIONS **1,160** CITATIONS
SEE PROFILE

Sushil Auluck
Indian Institute of Technology Kanpur
313 PUBLICATIONS **3,088** CITATIONS
SEE PROFILE

THE JOURNAL OF PHYSICAL CHEMISTRY B

Article

pubs.acs.org/JPCB

Optical Spectra and Band Structure of $Ag_xGa_xGe_{1-x}Se_2$ (x = 0.333, 0.250, 0.200, 0.167) Single Crystals: Experiment and Theory

A. H. Reshak,*[,†,‡] O. V. Parasyuk,[§] A. O. Fedorchuk,[∥] H. Kamarudin,[‡] S. Auluck,[⊥] and J. Chyský[#]

[†]New Technologies - Research Center, University of West Bohemia, Univerzitni 8, 306 14 Pilsen, Czech Republic

[‡]Center of Excellence Geopolymer and Green Technology, School of Material Engineering, University Malaysia Perlis, 01007 Kangar, Perlis, Malaysia

[§]Department of Inorganic and Physical Chemistry, Eastern European National University, 13 Voli Avenue, 43025 Lutsk, Ukraine

[∥]Department of Inorganic and Organic Chemistry, Lviv National University of Veterinary Medicine and Biotechnologies, 50 Pekarska Street, 79010 Lviv, Ukraine

[⊥]Council of Scientific and Industrial Research - National Physical Laboratory, Dr. K S Krishnan Marg, New Delhi 110012, India

[#]Department of Instrumentation and Control Engineering, Faculty of Mechanical Engineering, CTU in Prague, Prague, Czech Republic

ABSTRACT: Theoretical and experimental studies of the $Ag_xGa_xGe_{1-x}Se_2$ (x = 0.333, 0.250, 0.200, 0.167) single crystals are performed. These crystals possess a lot of intrinsic defects which are responsible for their optoelectronic features. The theoretical investigations were performed by means of DFT calculations using different exchange-correlation potentials. The experimental studies were carried out using the modulated VUV ellipsometry for dielectric constants and birefringence studies. The comparison of the structure obtained from X-ray with the theoretically optimized structure is presented. The crucial role of the intrinsic defect states is manifested in the choice of the exchange correlation potential used. The data may be applicable for a large number of the ternary chalcogenides which are sensitive to the presence of the local disordered states near the band edges.

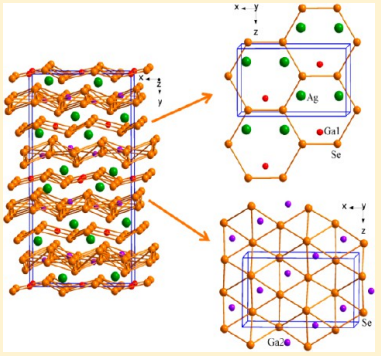

1. INTRODUCTION

The studies of the ternary chalcogenide crystals have shown that these crystals have a great potential for the optoelectronic and infrared nonlinear optics[1] especially in the infrared spectral range. One of the ways to improve their optoelectronic features is photoinduced treatment of their intrinsic defect states. Even though a lot of data exists, there seems to be a lack of any analysis of the band structure, charge density, and linear optical properties. Following our evaluations, only coexistence of the excellent properties of the chalcogenides with respect to photoinduced susceptibilities together with the good properties of the Ag ions could give excellent materials which result in good photoinduced features and conductivities. In this work, we will focus our attention on this class of materials. A theoretical consideration of these factors and a comparison of the principal results allow us to understand the contributions to the observed optical susceptibilities as manifested in the experimental data. In the present work, we report results of comprehensive DFT studies of the investigated crystals using the different exchange correlation potentials seeking the optimal results to achieve a sufficient agreement with the principal experimental data. Moreover, the comparison with the experiments shows how crucial the role of the intrinsic defect trapping states[2] is in defining the many properties of these materials. We have chosen the $Ag_xGa_xGe_{1-x}Se_2$ (x = 0.333, 0.250, 0.200, 0.167) single crystals covering both some previously studied crystals[3] as well the new ones. A consideration of a large range of the crystals can give a picture about the possible band structure and electronic parameters defining the optoelectronic features.

In section 2, we present principal experimental methods and crystal structures. Section 3 describes calculation methods. Section 4 presents the results of the band structure calculations. Section 5 presents some comparison of optical functions with experimental data. Finally, section 6 summarizes the results.

2. EXPERIMENTAL METHODS

The crystal structure of the sulfur-containing compounds $AgGaGeS_4$ (SG $Fdd2$, a = 12.028, b = 22.918, c = 6.874 Å) was first deciphered by Pobedimskiya et al.[4] At the same time, for similar selenium compounds $AgGaGeSe_4$, Hughes et al.[5] proposed a tetragonal space group I-42d with unit cell parameters a = 5.826 and c = 10.38 Å. Later, in the investigation of the phase diagram $AgGaSe_2$–$GeSe_2$,[6] it has been shown that this compound is part of a solid solution based on $AgGaSe_2$ and really has a tetragonal structure. However, the system detected a new γ-phase ($Ag_xGa_xGe_{1-x}Se_2$), which has a

Received: November 1, 2013
Published: November 12, 2013

   dx.doi.org/10.1021/jp410786w | J. Phys. Chem. B 2013, 117, 15220–15231

large homogeneity range and is indexed in the orthorhombic structure of the compound $AgGaGeS_4$ with cell parameters a = 12.4108, b = 23.7787, and c = 7.1353 Å (for x = 0.167). The detailed structure of the crystal-chemical analysis was not carried out by the authors. In the Olekseyuk et al. work,[7] some attention is paid to the mechanism of formation of solid solutions, although complete data of crystal research, in particular the atomic coordinates, are not given. The titled crystals were synthesized by a method described in ref 8.

X-ray studies of four compositions of the solid solution $Ag_xGa_xGe_{1-x}Se_2$, as well as alloys with the replacement of one of its components, were performed on a DRON 4-13 diffractometer with Cu Kα radiation. An array of X-ray diffraction reflections was obtained in the range 10−100° in increments equal to 0.02° and 20 at each point. Calculation of the crystal structure was performed using the software package CSD.[3] The basic model for the calculation of the crystal structure of the phase structure of the compound served $AgGaGeS_4$.[4] In the three crystallographic positions of sulfur, 16b possesses selenium. Positions of p-bits and pieces are equivalent in the two compounds—a statistical arrangement of two positions 8a and 16b. Proportion statistics Ga/Ge launch pad wandered original formula based compounds. The Silver position (16b) is also equivalent to and is characterized by underemployment. In each case, the initial filling of the position wandered silver compounds based on the formula and refined in the process. Calculation at the baseline led to satisfactory results, as indicated by the values of the factors of reliability and difference diffraction profiles. The obtained values of the unit cell parameters of phase $Ag_xGa_xGe_{1-x}Se_2$ interatomic distances Kat−An are shown in Table 1, and agree well with the previous data.[2,3,6,7] As the table shows, the crystallographic positions of the atoms in the structure are filled chalcogen four compositions are always fully considered, and differ in the position of the fill factor of the metal component and the ratio of p-atoms in position 16b element i 8a. Somewhat higher values of thermal parameters of silver atoms were observed in all four related structures. This could be due to the deficiency of their crystallographic positions and the high mobility of the atoms themselves.

Table 1. The Unit Cell Parameters, Reliability Factors, and Interatomic Distances of Atoms in Solid $Ag_xGa_xGe_{1-x}Se_2$

	x = 0.333 $AgGaGe_2Se_6$	x = 0.250 $AgGaGe_3Se_8$	x = 0.200 $AgGaGe_4Se_{10}$	x = 0.167 $AgGaGe_5Se_{12}$
a (Å)	12.4967(6)	12.4423(6)	12.4126(5)	12.4107(6)
b (Å)	23.905(1)	23.820(1)	23.7689(9)	23.767(1)
c (Å)	7.1420(3)	7.1403(3)	7.1384(3)	7.1364(3)
V (Å^3)	2133.5(3)	2116.3(3)	2106.1(3)	2105.0(3)
density (g/cm^3)	4.9592(7)	4.8349(7)	4.7589(6)	4.6946(7)
R_I	0.0497	0.0477	0.0436	0.0770
R_P	0.1257	0.1153	0.1051	0.1567
texture axis and parameter	[130], 1.36(3)	[130], 1.41(3)	[130], 1.14(2)	[130], 2.73(6)
Ag−Se2	2.591(5)	2.522(5)	2.434(6)	2.455(9)
Ag−Se2	2.613(6)	2.543(5)	2.591(5)	2.580(9)
Ag−Se3	2.768(5)	2.768(5)	2.716(5)	2.796(9)
Ag−Se1	2.902(6)	3.056(5)	3.138(6)	2.986(9)
Ga1−Se1	2.381(4)[a]	2.355(3)[b]	2.371(2)[c]	2.367(3)[d]
Ga1−Se2	2.406(3)	2.376(2)	2.356(2)	2.375(3)
Ga2−Se1	2.345(5)[a]	2.367(3)[b]	2.369(2)[c]	2.325(3)[d]
Ga2−Se2	2.346(4)	2.381(3)	2.382(3)	2.419(4)
Ga2−Se3	2.362(3)	2.328(3)	2.340(2)	2.358(3)
Ga2−Se3	2.390(5)	2.394(3)	2.382(3)	2.375(3)

[a]0.333 Ga + 0.667 Ge. [b]0.250 Ga + 0.750 Ge. [c]0.200 Ga + 0.800 Ge. [d]0.167 Ga + 0.833 Ge.

The VUV data were performed using the VUV monochromator with a spectral resolution of about 7.0 A/mm. The modulated method was performed by grating with 600 mm^{-1} with a spectral resolution of 1 nm in the spectral range from 5.0 eV up to 10.0 eV using a setup similar to that described in ref 9. Varying the wavelength the studies was performed for the detection of the spectral positions for the first reflected spectral maximum. The dielectric susceptibilities were measured using the static condensator method. Birefringence was measured by the method of Senarmont[10] with an accuracy of about 10^{-6}. Experimental, calculated, and difference X-ray diffraction spectra shown in Figure 1 indicate good agreement. Atomic coordinates and isotropic thermal parameters of the compounds are listed in Table 2.

The crystal structure of $Ag_xGa_xGe_{1-x}Se_2$ can be regarded as laying the blocks along the [010] plane, as shown in Figure 2. These blocks are formed by deformed chalcogen atoms. Moreover, the layers are similar to the layers in the structure of sphalerite and wurtzite (Figure 3), while the layers can be seen as a result of the removal of individual atoms from layers of upper levels. This view suggests that the anionic sublattice structure can be seen as a result of the removal of individual atoms with the anionic sublattice type sphalerite and wurtzite with the strain changing the original structure. In other words, we have a defected structure or a structure with intrinsic defects. The thickness of the unit value is measured between the centers of the outer layer of atoms (Figure 2) and is very different for bad blocks on it is less than half of the order. This may indicate competition between deformation changes and the removal of the atoms of the anion. The defective layer is less deformed. As for atoms of the cation, the location of p-elements in the structure $Ag_xGa_xGe_{1-x}Se_2$ and compounds $GeSe_2$[11] obtained at high pressures is the same type of rice, Figure 4. Both structures can be seen as laying the tetrahedra around the atoms of p-element. Channels formed by inter-tetrahedral space in the case of a structure $Ag_xGa_xGe_{1-x}Se_2$ are filled with silver atoms. The presence of the atoms in the channels obviously leads to the deformation of the transformation joints cut $AgGaSe_2$−$GeSe_2$, and the relationship of these structures may indicate only the presence of the above-mentioned channels, which in the case of $GeSe_2$ are two-dimensional, along the crystallographic axes x and y. Silver atoms form around a few deformed tetrahedra of selenium atoms, connected vertices, and form sophisticated bonds (bands) along [00z], as shown in Figure 4. The gaps between these bands are filled by atoms of p-elements.

3. COMPUTATIONAL DETAILS

We have employed the all-electron-full potential linearized augmented plane wave (FP-LAPW) method to calculate the electronic band structure, total and partial density of states, and linear optical properties of $Ag_xGa_xGe_{1-x}Se_2$ (x = 0.333, 0.250, 0.200, 0.167) single crystals. It is a continuous series of compounds; thus, as a prototype, we will show the results of the first and the last compound. FP-LAPW is based on density functional theory (DFT) as implemented in the WIEN2K code.[12] The DFT calculations are carried out on the minimized

dx.doi.org/10.1021/jp410786w | J. Phys. Chem. B 2013, 117, 15220−15231

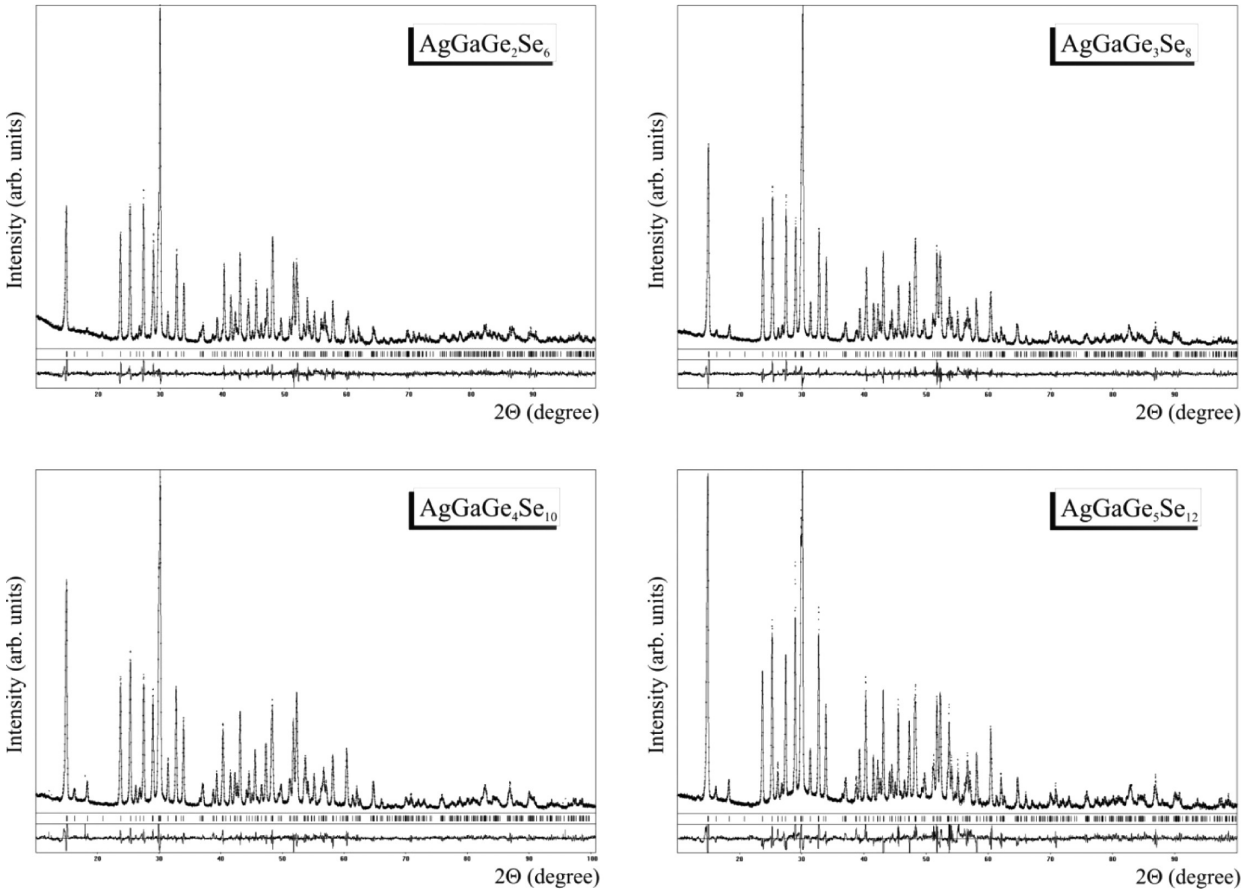

Figure 1. Experimental, theoretical, and difference difractograms of $Ag_xGa_xGe_{1-x}Se_2$ alloys.

structure of $Ag_xGa_xGe_{1-x}Se_2$. The structure we have chosen for DFT calculations has intrinsic defects. We have relaxed the geometry by minimizing the forces acting on each atom. We assume that the structure is totally relaxed when the forces on each atom reach values less than 1 mRy/a.u. The self-consistent field tolerance is 10^{-4} Ry. The electronic exchange-correlation energy is treated by the local density approximation (LDA) Ceperley–Alder (CA) approach,[13] the generalized gradient approximation (GGA),[14] and the Engel–Vosko generalized gradient approximation (EVGGA)[15] which is more superior to local density approximation (LDA). We have used a modified Becke–Johnson potential (mBJ)[16] to obtain a better band gap value that is mostly underestimated by LDA and GGA. The structure of $Ag_xGa_xGe_{1-x}Se_2$ is orthorhombic with space group *Fdd2* (No. 43). The atomic positions and lattice constants are presented in Tables 1 and 2.

The self-consistency is obtained using 35 **k**-points in the irreducible Brillouin zone (IBZ). For calculating the total and the angular momentum decomposition of the atoms projected electronic density of states, a mesh of 400 **k**-points was used, whereas for the optical properties 600 **k**-points in the IBZ were used.

4. RESULT AND DISCUSSION

4.1. Electronic Band Structure and Density of States.

The calculated electronic band structures of $Ag_xGa_xGe_{1-x}Se_2$ using LDA, GGA, EVGGA, and mBJ are presented in Figure 5. It is clear that the conduction band minimum (CBM) is situated at the center of the BZ and the valence band maximum (VBM) at the L point of the BZ. These figures suggest that the investigated compounds are an indirect band gap between 1.4 and 1.6 eV. The total density of states are calculated using LDA, GGA, EVGGA, and mBJ, as illustrated in Figure 6a and b. We find that mBJ produces better band splitting and hence better band gaps. Thus, we have selected to show the calculated partial density of states obtained by using mBJ (see Figure 6 c–n). We have found that the CB is formed prevailingly from Ag-s/p, Ge-s/p/d, Ga-s/p, and Se-p/d states. The upper VB is formed by Ag-s/p/d, Ge-p/d, Ga-p/d, and Se-p/d states. To clarify the contribution of each orbital of these atoms, we investigate the angular momentum decomposition of the atoms projected density of states (PDOS). The PDOS helps to identify the angular momentum character of the various structures; the peaks centered from −13.0 to −12.0 eV are due to the maximum contribution of Se-s and Ga-d states with a small contribution of Ge-p/d state; at this energy limit (i.e., −13.0 and −12.0 eV), there is a strong hybridization between Ga-s and Ge-p states and also between Ga-d and Ge-p states. The peaks lying between −6.5 and 0.0 eV for the compounds consist of Ag-d, Ga-s, and Se-p states with minimum contribution of Ge-p and Ga-d. The structures from 1.0 up to 7.0 eV are due to the major contribution of Ga-s/p and Ge-s/p states; we would like to mention that at this energy limit there is a strong hybridization between Ga-p and Ge-p states. The structures at higher energies are due to the Se-d/p and Ge-p/d states. The difference between the structures of the two compounds is that, for the $AgGaGe_2Se_6$ compound, the peaks at −9.0 and −8.0 eV are due to the maximum contribution of Ge-s state along with a small contribution of Ga-s and Se-p and also at this energy range there exists a strong hybridization

dx.doi.org/10.1021/jp410786w | J. Phys. Chem. B 2013, 117, 15220–15231

Table 2. The Atomic Coordinates for the Structures $Ag_xGa_xGe_{1-x}Se_2$

atom	position	x/a	y/b	z/c	B(is/eq)	occup.
			$AgGaGe_2Se_6$ (x = 0.333)			
Ag	16*b*	0.0780(3)	0.2096(2)	0.7278(8)	4.9(2)	0.500
Ga1	8*a*	0	0	0.0000	2.17(14)	1*
Ga2	16*b*	0.1232(2)	0.1136(1)	0.2710(5)	1.84(10)	1*
Se1	16*b*	0.2009(2)	0.1742(1)	0.0516(6)	1.14(8)	1
Se2	16*b*	0.1586(2)	0.0214(1)	0.1770(6)	1.79(9)	1
Se3	16*b*	0.1904(2)	0.11957(10)	0.5837(5)	1.09(8)	1
* 0.333 Ga + 0.667 Ge						
			$AgGaGe_3Se_8$ (x = 0.250)			
Ag	16*b*	0.0692(4)	0.2101(2)	0.7111(7)	7.3(2)	0.375
Ga1	8*a*	0	0	0.0017(4)	1.44(10)	1*
Ga2	16*b*	0.1226(2)	0.11358(9)	0.2736(3)	1.61(7)	1*
Se1	16*b*	0.2011(2)	0.17535(8)	0.0530(3)	1.29(6)	1
Se2	16*b*	0.1599(2)	0.0206(1)	0.1701(3)	2.35(7)	1
Se3	16*b*	0.1914(2)	0.12057(8)	0.5859(3)	0.94(6)	1
* 0.250 Ga + 0.750 Ge						
			$AgGaGe_4Se_{10}$ (x = 0.200)			
Ag	16*b*	0.0690(4)	0.2101(2)	0.6976(8)	6.9(2)	0.300
Ga1	8*a*	0	0	0.0079(4)	1.44(8)	1*
Ga2	16*b*	0.1266(2)	0.36308(8)	0.5265(3)	1.37(6)	1*
Se1	16*b*	0.0496(2)	0.42541(7)	0.3050(2)	1.44(5)	1
Se2	16*b*	0.0900(1)	0.26975(9)	0.4229(3)	2.17(6)	1
Se3	16*b*	0.0593(2)	0.37098(7)	0.8379(2)	0.80(5)	1
* 0.200 Ga + 0.800 Ge						
			$AgGaGe_5Se_{12}$ (x = 0.167)			
Ag	16*b*	0.0672(7)	0.2101(4)	0.7258(12)	7.3(4)	0.250
Ga1	8*a*	0	0	0.0004(4)	0.70(11)	1*
Ga2	16*b*	0.1241(2)	0.1133(1)	0.2724(4)	1.40(8)	1*
Se1	16*b*	0.1996(2)	0.1742(1)	0.0540(3)	2.28(8)	1
Se2	16*b*	0.1603(2)	0.0179(1)	0.1722(3)	1.89(7)	1
Se3	16*b*	0.1898(2)	0.12114(10)	0.5838(3)	0.92(7)	1
* 0.167 Ga + 0.833 Ge						

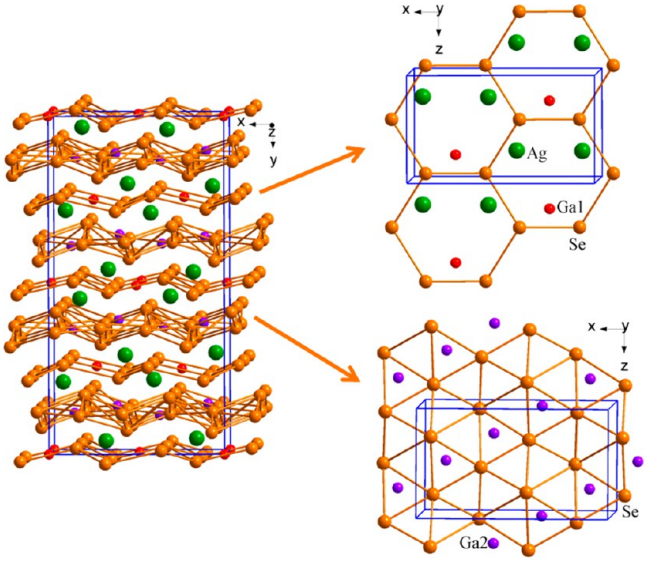

Figure 2. The crystalochemistry of chalcogens in the structure $Ag_xGa_xGe_{1-x}Se_2$.

between Ga-s and Se-p states, and for the $AgGaGe_5Se_{12}$ compound, the peaks at −8.0 and −6.5 eV are due to the Se-p state.

Generally, the lead ions cause a huge additional polarization which favors nonlinear optical features.[17−19] Following the data concerning the band structure of the chalcogenides, it is clear that their valence band is formed prevailingly by the bonded p-originated chalcogen orbitals.[20−22] The presence of silver usually gives some additional effects and first of all the ionic conductivity[23] as well as additional trapping levels within the energy gap.[24]

From the calculated PDOS of Ag-s/p/d, Se-p, Ga-s/p, and Ge-s/p states (Figure 6c−n), we can identify the origin of the chemical bonding. The valence band from Fermi energy down to −8.0 eV for $AgGaGe_2Se_6$ ($AgGaGe_5Se_{12}$) is mainly originated from Ag-d states with a magnitude of about 8.5 e/eV (6.8 e/eV), Ga-s states 1.7 e/eV (1.4 e/eV), Ge-s states 0.4 e/eV (0.4 e/eV), Se-p states 0.65 e/eV (0.9 e/eV), Ge-s states 1.1 e/eV (2.0 e/eV), Ge-p states 0.4 e/eV (0.55 e/eV), Ag-s states 0.12 e/eV(0.1 e/eV), Ag-p states 0.11 e/eV (0.1 e/eV), and Ga-p states 0.47 e/eV (0.5 e/eV). The states Ag-s/p/d, Se-p, Ga-s/p, and Ge-s/p present a strong hybridization and hence a covalent bonding.

4.2. Effective Mass. We have calculated the effective mass of electrons (m_e^*) from the band structure; these values were estimated from the curvature of CBM, band no. 155 for $AgGaGe_2Se_6$ and band no. 147 for $AgGaGe_5Se_{12}$. The diagonal elements of m_e^* for the electrons in the CB are calculated in Γ → L direction in k space using the expression

$$\frac{1}{m_e^*} = \frac{1\partial^2 E(k)}{\hbar^2 \partial k^2} \quad (1)$$

dx.doi.org/10.1021/jp410786w | J. Phys. Chem. B 2013, 117, 15220−15231

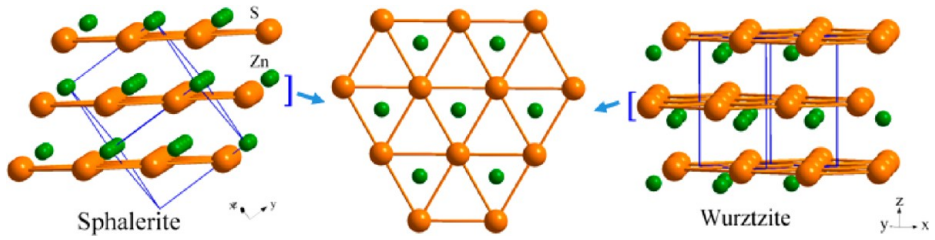

Figure 3. The structure of sphalerite and wurtzite for the given structural motifs.

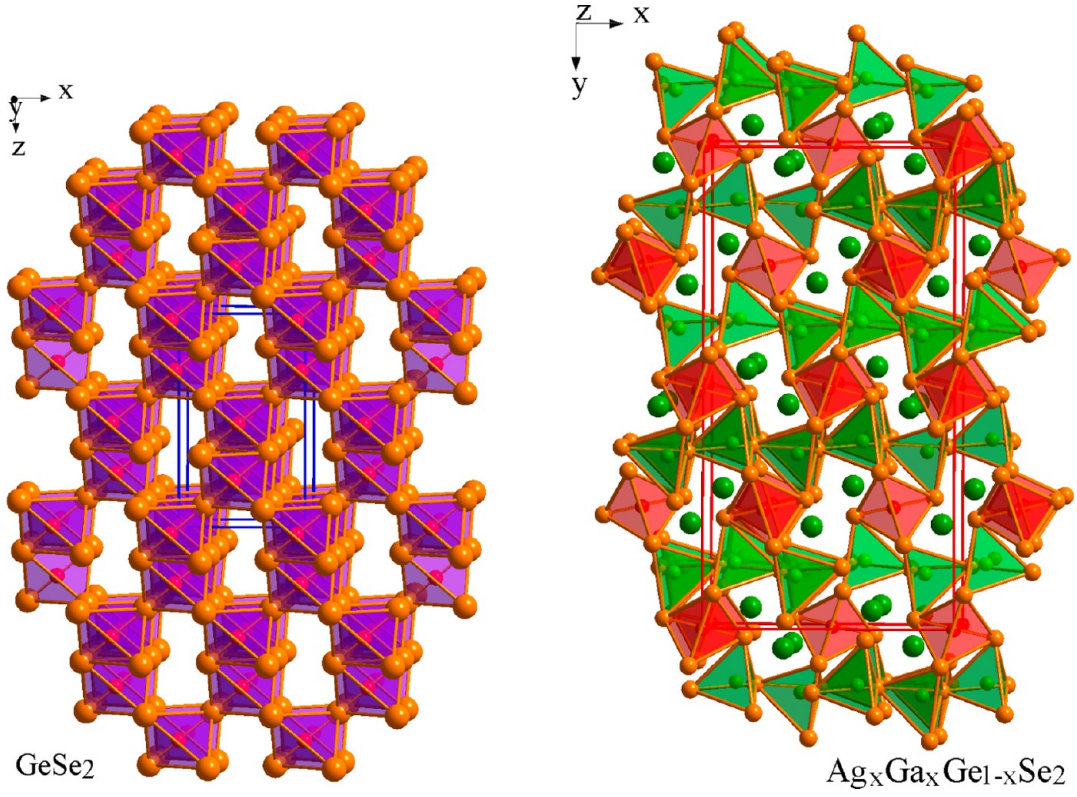

Figure 4. Packing of $GeSe_4$ tetrahedra (blue) in the structure of $GeSe_2$ and Ga_2Se (green) and Ga_1Se_4 (red) for compounds $Ag_xGa_xGe_{1-x}Se_2$.

The effective mass of electron is determined by fitting the electronic band structure to a parabolic function (eq 1) in the first BZ using the EVGGA approach. The effective mass of electron for the symmetry is obtained from the curvature of the CB at the Γ point. The calculated electron effective mass ratio (m_e^*/m_e) for $AgGaGe_2Se_6$ and $AgGaGe_5Se_{12}$ in the Γ → L direction is 0.0452 and 0.0397. It is obvious that the calculated value of $AgGaGe_2Se_6$ is larger than the $AgGaGe_5Se_{12}$ values. Because the parabolic curvature of $AgGaGe_5Se_{12}$ is greater than that of $AgGaGe_2Se_6$, we know that the effective mass is inversely proportional to the curvature. We have also calculated the effective mass of the heavy holes and light holes. The calculated valves for heavy holes and light holes for $AgGaGe_2Se_6$ ($AgGaGe_5Se_{12}$) compounds are 0.0199 and 0.033 (0.2620 and 0.0187).

5. OPTICAL PROPERTIES: DFT SIMULATIONS AND COMPARISON WITH EXPERIMENT

The calculated real and imaginary parts of the dielectric function for $Ag_xGa_xGe_{1-x}Se_2$ as a function of the photon energy were displayed in Figure 7a–d. The dielectric function $\varepsilon = \varepsilon_1 + i\varepsilon_2$ spectra will help in accounting for the optical transitions in $Ag_xGa_xGe_{1-x}Se_2$. The imaginary part of the dielectric function $\varepsilon_2(\omega)$ was calculated from the direct interband transitions using the expression given in ref 25:

$$\varepsilon_2(\omega) = \left(\frac{4\pi^2 e^2}{m^2\omega^2}\right)\sum_{i,j}\int \langle i|M|j\rangle^2 f_i(1-f_j)\delta(E_f - E_i - \omega)\,\mathrm{d}^3k$$

The real part $\varepsilon_1(\omega)$ can be derived from the imaginary part by means of the Kramers–Kronig relation:[26]

$$\mathrm{Re}[\varepsilon(\omega)] = \varepsilon_1(\omega) = 1 + \frac{2}{\pi}\mathrm{P}\int_0^\infty \frac{\omega'\mathrm{Im}\,\varepsilon(\omega')}{\omega'^2 - \omega^2}\,\mathrm{d}\omega'$$

The investigated $Ag_xGa_xGe_{1-x}Se_2$ compounds have orthorhombic symmetry. This symmetry allows only three nonzero components $\varepsilon_2^{xx}(\omega)$, $\varepsilon_2^{yy}(\omega)$, and $\varepsilon_2^{zz}(\omega)$ of the second-order dielectric tensor, which correspond to an electric field perpendicular and parallel to the **c**-axis. These are the imaginary parts of the frequency-dependent dielectric function. The calculated imaginary parts for the $AgGaGe_2Se_6$ and $AgGaGe_5Se_{12}$ compounds are shown in Figure 7a and b. As previewed from the figure, the calculated compounds have various optical spectra as we increase the concentration of Ge and Se. This is approved to the statistic that there is a small difference in the

dx.doi.org/10.1021/jp410786w | J. Phys. Chem. B 2013, 117, 15220–15231

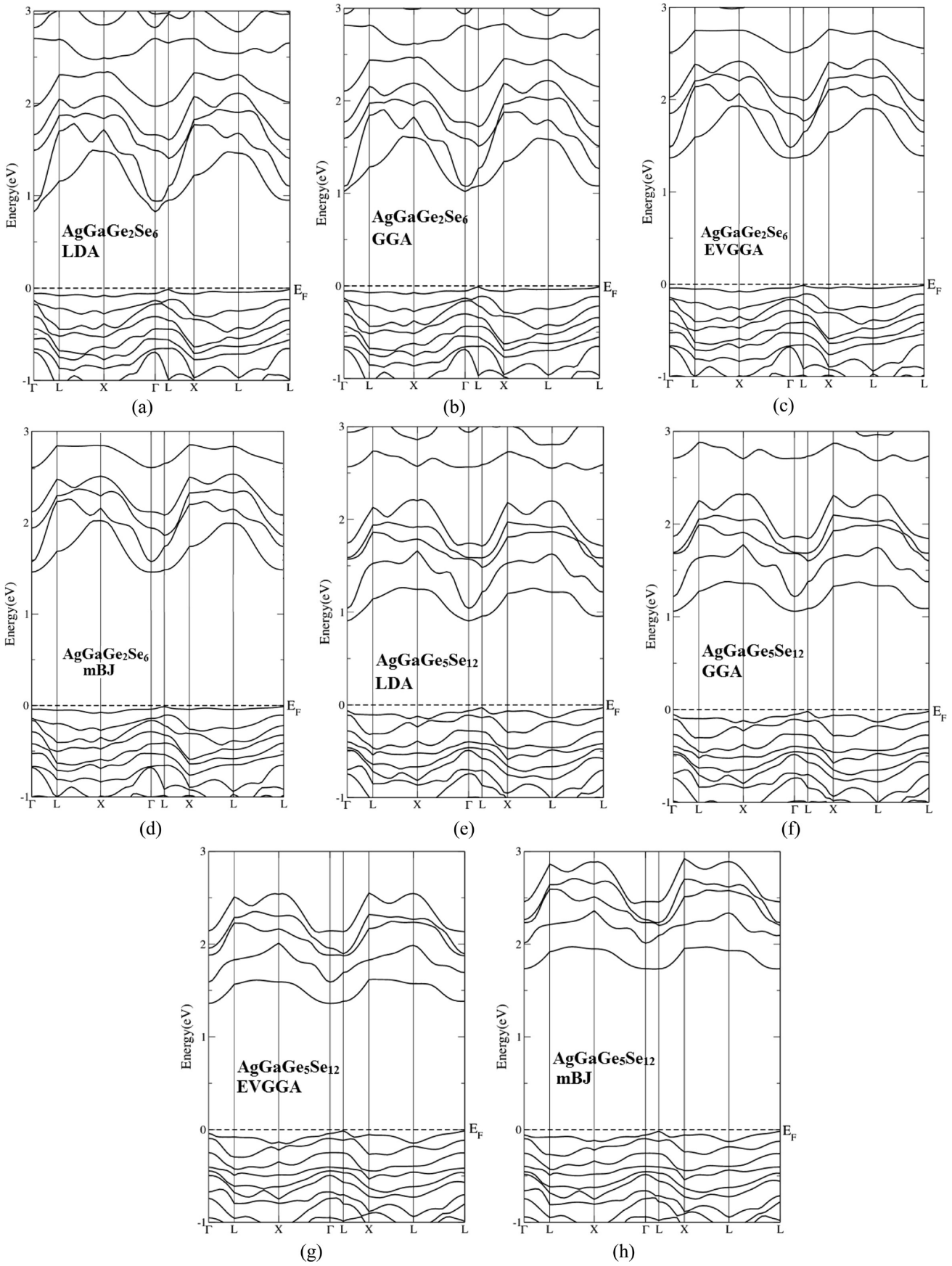

Figure 5. Calculated band structures using LDA, GGA, EVGGA, and mBJ for $AgGaGe_2Se_6$ and $AgGaGe_5Se_{12}$.

dx.doi.org/10.1021/jp410786w | J. Phys. Chem. B 2013, 117, 15220−15231

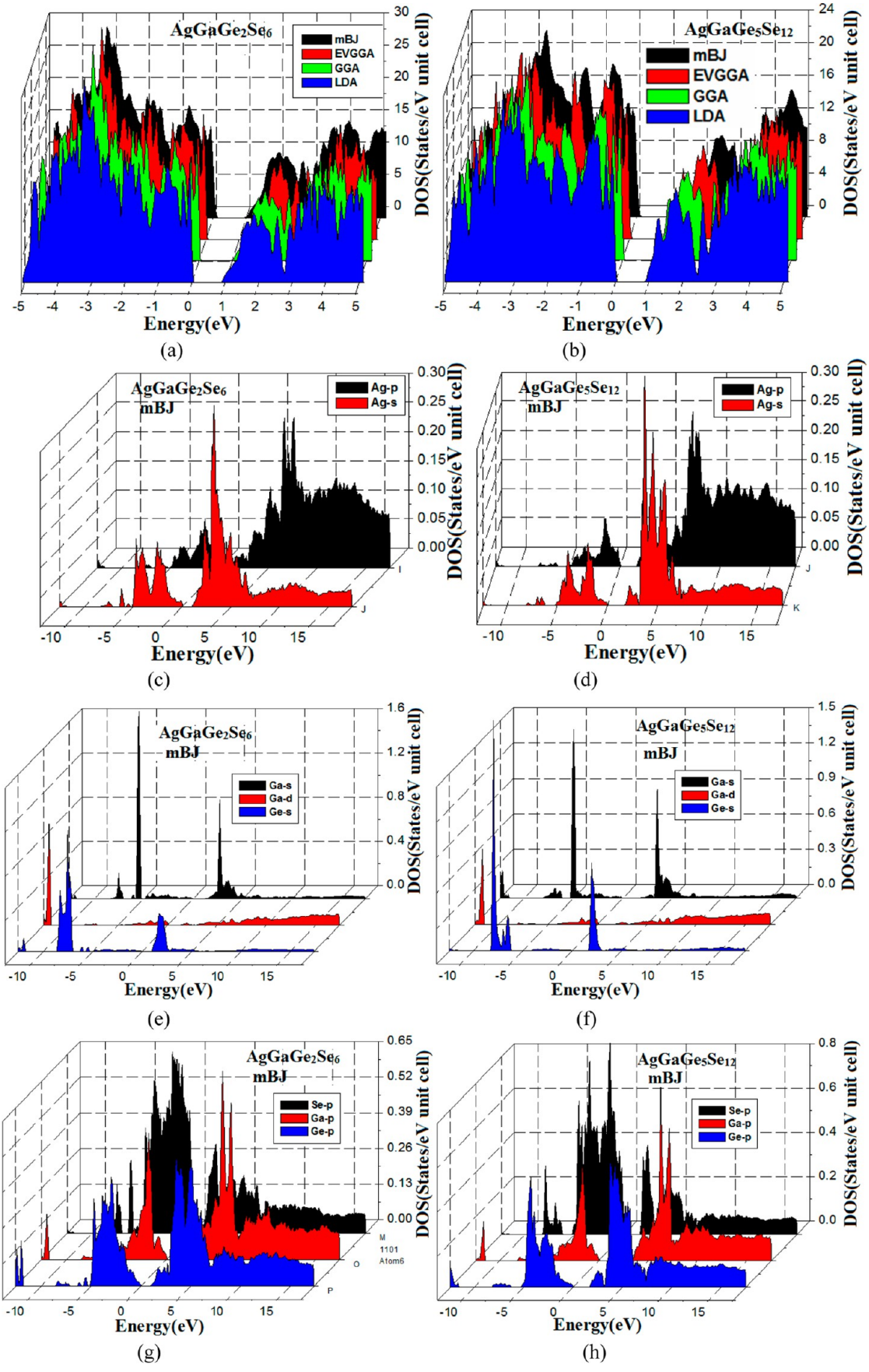

Figure 6. continued

dx.doi.org/10.1021/jp410786w | J. Phys. Chem. B 2013, 117, 15220−15231

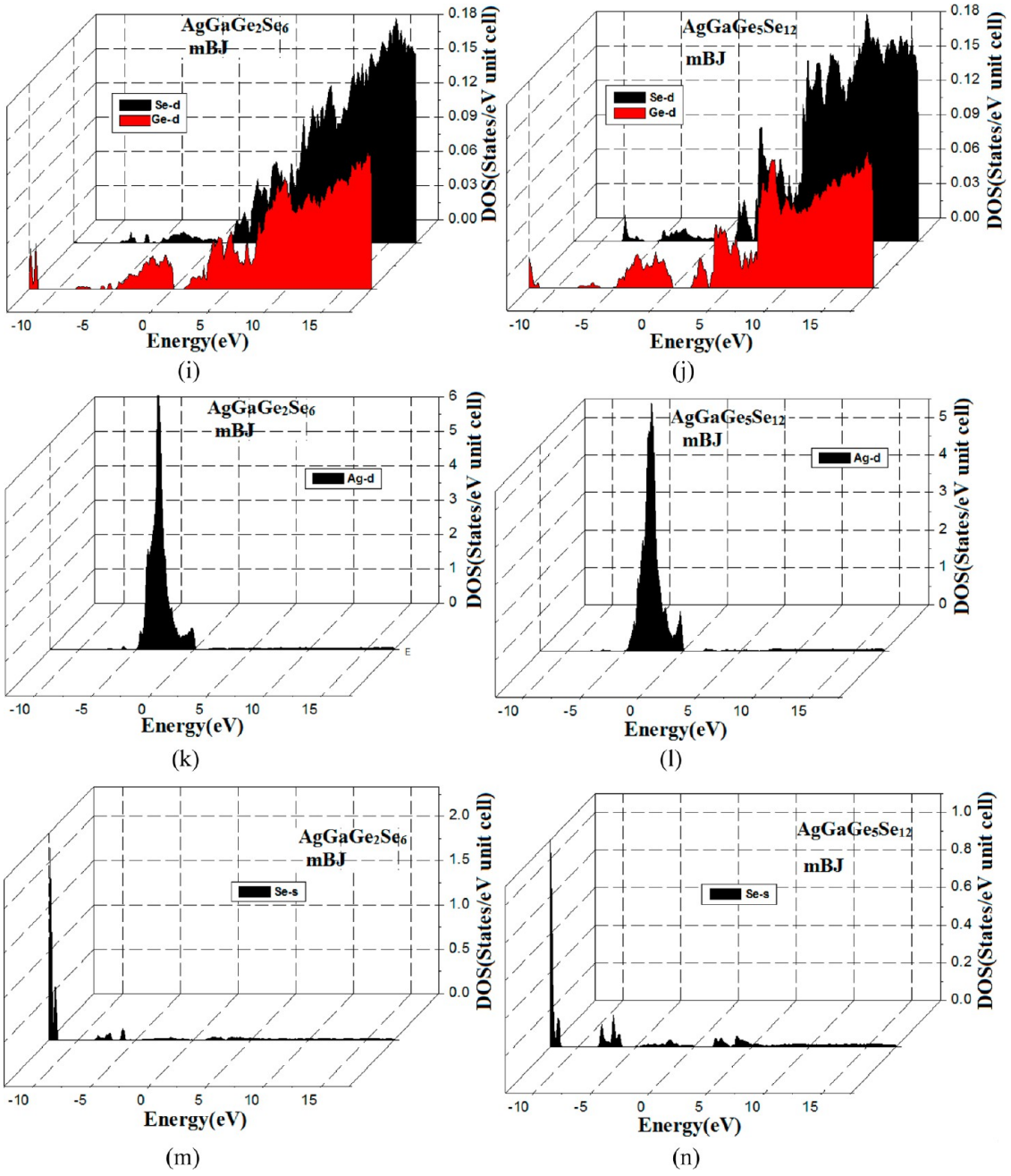

Figure 6. Calculated total density of states (TDOS) using LDA, GGA, EVGGA, and mBJ along with the partial density of states (PDOS). We have presented the results of PDOS only by using mBJ for $AgGaGe_2Se_6$ and $AgGaGe_5Se_{12}$.

band structures of these compounds. This originates the changes in the optical transitions in fluctuations of the peak heights and positions.

We noticed that in the $AgGaGe_2Se_6$ compound at low energy, i.e., 2.5−5 eV, there is a considerable anisotropy between the three components $\varepsilon_2^{xx}(\omega)$, $\varepsilon_2^{yy}(\omega)$, and $\varepsilon_2^{zz}(\omega)$, while from 5.0 eV to higher energies there is isotropy between the three spectra. By increasing the concentration of Ge and Se, it causes a shift of the entire structures to higher energies and drops all peak heights. The calculated three $\varepsilon_2^{xx}(\omega)$, $\varepsilon_2^{yy}(\omega)$, and $\varepsilon_2^{zz}(\omega)$ components of the $AgGaGe_5Se_{12}$ compound show considerable anisotropy between 5.0 and 8.0 eV. It is clear from Figure 7a and b that the anisotropy between the three optical components $\varepsilon_2^{xx}(\omega)$, $\varepsilon_2^{yy}(\omega)$, and $\varepsilon_2^{zz}(\omega)$ is corresponding to different polarization. The peak maxima are located at 9.75, 9.53, and 10.34 eV for $\varepsilon_2^{xx}(\omega)$, $\varepsilon_2^{yy}(\omega)$, and $\varepsilon_2^{zz}(\omega)$ of $AgGaGe_2Se_6$ and at 8.41, 8.61, and 8.76 eV for $\varepsilon_2^{xx}(\omega)$, $\varepsilon_2^{yy}(\omega)$, and $\varepsilon_2^{zz}(\omega)$ of $AgGaGe_5Se_{12}$. The corresponding values obtained from the UV-reflection using a VUV monochromator have shown that maxima were equal to 10.2, 10.02, and 10.24 eV for $\varepsilon_2^{xx}(\omega)$, $\varepsilon_2^{yy}(\omega)$, and $\varepsilon_2^{zz}(\omega)$ of $AgGaGe_2Se_6$. For $AgGaGe_5Se_{12}$, the corresponding values found from the UV-reflection using a VUV monochromator have shown that maxima were equal to 9.02, 9.12, and 9.34 eV for $\varepsilon_2^{xx}(\omega)$, $\varepsilon_2^{yy}(\omega)$, and $\varepsilon_2^{zz}(\omega)$.

The results of our calculated real parts $\varepsilon_1^{xx}(\omega)$, $\varepsilon_1^{yy}(\omega)$, and $\varepsilon_1^{zz}(\omega)$ are shown in Figure 7c and d. The calculated value of $\varepsilon_1^{xx}(0)$ is 9.303 (6.621), $\varepsilon_1^{yy}(0)$ is 9.057 (6.536), and $\varepsilon_1^{zz}(0)$ is 8.987 (6.527) for $AgGaGe_2Se_6$ ($AgGaGe_5Se_{12}$). The uniaxial anisotropy $\delta\varepsilon = \lfloor(\varepsilon_0^{\parallel} - \varepsilon_0^{\perp})/\varepsilon_0^{tot}\rfloor$ is about −0.0077 (−0.00211)

dx.doi.org/10.1021/jp410786w | J. Phys. Chem. B 2013, 117, 15220−15231

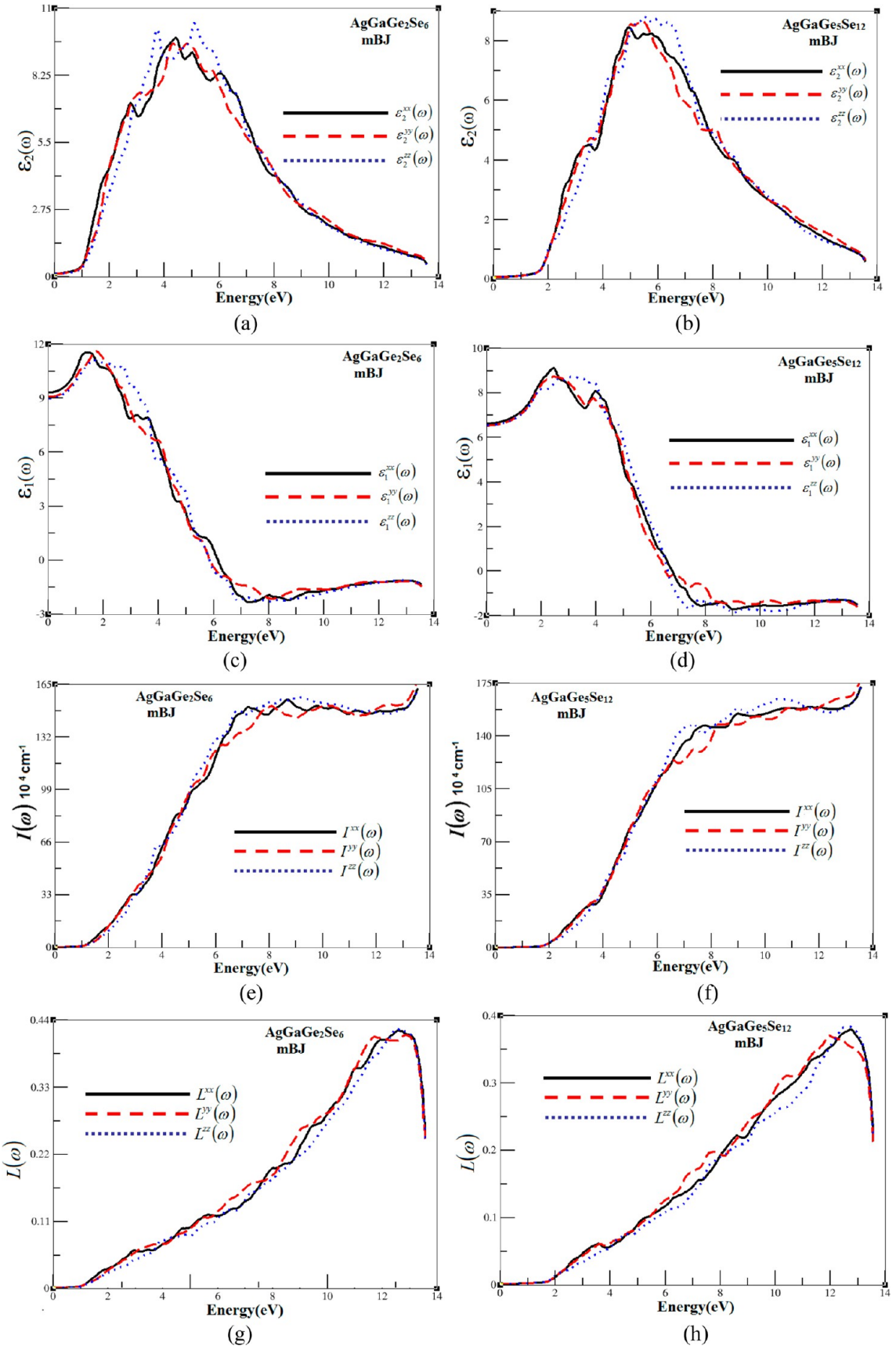

Figure 7. continued

dx.doi.org/10.1021/jp410786w | J. Phys. Chem. B 2013, 117, 15220−15231

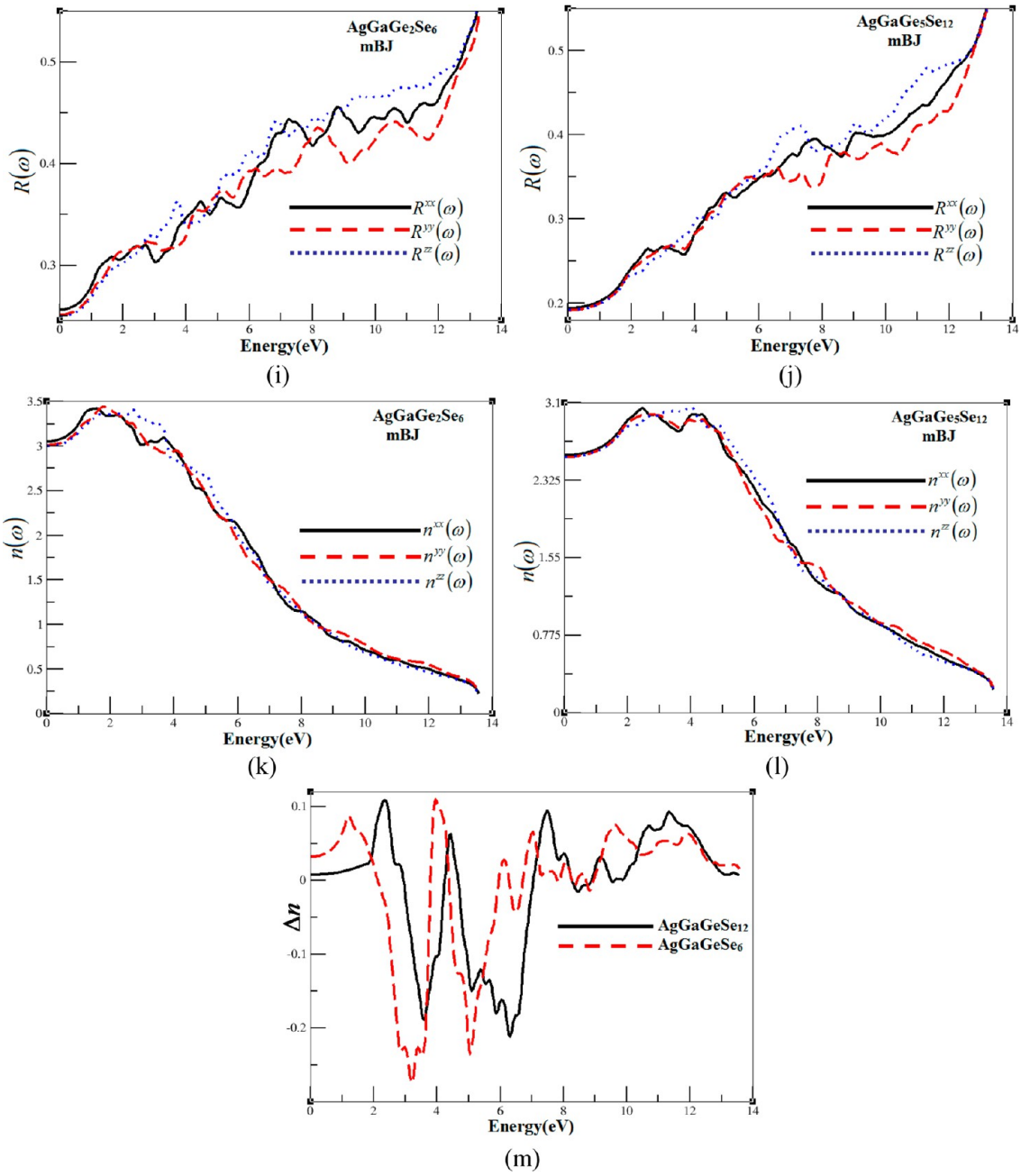

Figure 7. (a, b) Calculated $\varepsilon_2^{xx}(\omega)$ (black solid curve), $\varepsilon_2^{yy}(\omega)$ (red dashed curve), and $\varepsilon_2^{zz}(\omega)$ (blue dotted curve) dispersion spectra using mBJ for $AgGaGe_2Se_6$ and $AgGaGe_5Se_{12}$. (c, d) Calculated $\varepsilon_2^{xx}(\omega)$ (black solid curve), $\varepsilon_2^{yy}(\omega)$ (red dashed curve), and $\varepsilon_2^{zz}(\omega)$ (blue dotted curve) spectra using mBJ for $AgGaGe_2Se_6$ and $AgGaGe_5Se_{12}$. (e, f) Calculated absorption coefficient $I^{xx}(\omega)$ (black solid curve), $I^{yy}(\omega)$ (red dashed curve), and $I^{zz}(\omega)$ (blue dotted curve) spectrum using mBJ for $AgGaGe_2Se_6$ and $AgGaGe_5Se_{12}$, the absorption coefficient in 10^4 cm^{-1}. (g, h) Calculated energy loss function $L^{xx}(\omega)$ (black solid curve), $L^{yy}(\omega)$ (red dashed curve), and $L^{zz}(\omega)$ (blue dotted curve) spectrum using mBJ for $AgGaGe_2Se_6$ and $AgGaGe_5Se_{12}$. (i, j) Calculated $R^{xx}(\omega)$ (black solid curve), $R^{yy}(\omega)$ (red dashed curve), and $R^{zz}(\omega)$ (blue dotted curve) using mBJ for $AgGaGe_2Se_6$ and $AgGaGe_5Se_{12}$. (k, l) Calculated refractive indices $n^{xx}(\omega)$ (black solid curve), $n^{yy}(\omega)$ (red dashed curve), and $n^{zz}(\omega)$ (blue dotted curve) spectrum using mBJ for $AgGaGe_2Se_6$ and $AgGaGe_5Se_{12}$. (m) Calculated birefringence $\Delta n(\omega)$ using mBJ for $AgGaGe_2Se_6$ and $AgGaGe_5Se_{12}$.

for $AgGaGe_2Se_6$ ($AgGaGe_5Se_{12}$), indicating anisotropy[24] exists between the dielectric function in these compounds.

Using the calculated dispersions of $\varepsilon_2(\omega)$ and $\varepsilon_1(\omega)$, one can evaluate other optical properties such as refractive index $n(\omega)$, absorption coefficient $I(\omega)$, reflectivity $R(\omega)$, and energy loss function $L(\omega)$. These are illustrated in Figure 7e–l. The absorption bands in the investigated compounds are due to the inter-ion transitions shown in Figure 7e and f. These figures show that $Ag_xGa_xGe_{1-x}Se_2$ single crystals exhibit absorption edges at the fundamental energy gaps and then rapidly increase to reach their maximum at the higher energies. There exists considerable anisotropy between $I^{xx}(\omega)$, $I^{yy}(\omega)$, and $I^{zz}(\omega)$ components at the energy range from 5.0 eV and above. Also, we have calculated the electron energy-loss function for $Ag_xGa_xGe_{1-x}Se_2$ single crystals, as shown in Figure 7g and h. The maximum peaks in the energy-loss function are associated with the existence of plasma oscillations. Parts i and j of Figure 7 show the calculated reflectivity spectra. These compounds

dx.doi.org/10.1021/jp410786w | J. Phys. Chem. B 2013, 117, 15220–15231

show low reflectivity at lower energies, which rapidly increases with increasing energies to reach its maximum values at 13.0 eV. Parts k and l of Figure 7 display the variation of refractive indices as a function of incident photon energy. We note that at low energy range the investigated materials show high refractive indices and then go to lower values at the high energies. The calculated nonzero tensor components of the static refractive index are 2.573 (3.050) for $n^{xx}(0)$, 2.555 (3.010) for $n^{yy}(0)$, and 2.556 (2.998) for $n^{zz}(0)$ of $AgGaGe_2Se_6$ ($AgGaGe_5Se_{12}$). The experimental values following the performed measurements of the dielectric constant tensor have given the corresponding values $n^{xx}(0)$ 3.25(2.92) and 3.23(2.87) for $n^{yy}(0)$ and $n^{zz}(0)$ of $AgGaGe_2Se_6$ ($AgGaGe_5Se_{12}$). Penn's model[27] shows that $\varepsilon_1(0)$ depends on the energy band gap of the material and $\varepsilon_1(0)$ is directly related to $n(0)$ by the relation $n(\omega) = (\varepsilon_1(0))^{1/2}$.

The three components of the refractive indices show considerable anisotropy along the spectral region and hence called birefringent. The birefringence is an important quantity to fulfill the phase-matching condition. It can be calculated from the parallel and perpendicular components of the refractive indices to the **c**-axis. Figure 7m represents the birefringence $\Delta n(\omega)$ for $Ag_xGa_xGe_{1-x}Se_2$. We find that the birefringence at zero energy $\Delta n(0)$ is 0.029 for $AgGaGe_2Se_6$ and 0.017 for $AgGaGe_5Se_{12}$. The experimental values were equal to 0.038 for $AgGaGe_2Se_6$ and 0.014 for $AgGaGe_5Se_{12}$. This magnitude may be a confirmation of the results obtained.[28] The principal role may be played by the intrinsic defects which is very high in these defects. The intrinsic defects are typical for the chalcogenide glasses, and they give from a huge number of defect states below the conduction band. The latter sub-bands cause additional polarization of the crystal during the phototreatment. Using their concentration by the laser annealing, one can obtain the changes of the corresponding parameters of the optical parameters up to 10−12% without the changes of the crystalline structure. However, more detailed analysis will be a subject of a separate work in the future.

6. CONCLUSIONS

We have obtained a reasonable agreement between the experimental data on the VUV ellipsemtric spectra for principal dielectric function peak positions and the refractive index magnitudes. The discrepancies are typical for the DFT calculations. The calculated nonzero tensor components of the static refractive index are 2.573 (3.050) for $n^{xx}(0)$, 2.555 (3.010) for $n^{yy}(0)$, and 2.556 (2.998) for $n^{zz}(0)$ of $AgGaGe_2Se_6$ ($AgGaGe_5Se_{12}$). The experimental values following the performed measurements of the dielectric constant tensor have given the corresponding values $n^{xx}(0)$ 325 (2.92) and 3.23 (2.87) for $n^{yy}(0)$ and $n^{zz}(0)$ of $AgGaGe_2Se_6$ ($AgGaGe_5Se_{12}$). The peak maxima are located at 9.75, 9.53, and 10.34 eV for $\varepsilon_2^{xx}(\omega)$, $\varepsilon_2^{yy}(\omega)$, and $\varepsilon_2^{zz}(\omega)$ of $AgGaGe_2Se_6$ and at 8.41, 8.61, and 8.76 eV for $\varepsilon_2^{xx}(\omega)$, $\varepsilon_2^{yy}(\omega)$, and $\varepsilon_2^{zz}(\omega)$ of $AgGaGe_5Se_{12}$. The corresponding values found from the UV-reflection using a VUV monochromator have shown that maxima were equal to 10.2, 10.02, and 10.24 eV for $\varepsilon_2^{xx}(\omega)$, $\varepsilon_2^{yy}(\omega)$, and $\varepsilon_2^{zz}(\omega)$ of $AgGaGe_2Se_6$. For $AgGaGe_5Se_{12}$, the corresponding values found from the UV-reflection using a VUV monochromator have shown that maxima were equal to 9.02, 9.12, and 9.34 eV for $\varepsilon_2^{xx}(\omega)$, $\varepsilon_2^{yy}(\omega)$, and $\varepsilon_2^{zz}(\omega)$. We find the traditional underestimations of the interband values during the DFT studies. The obtained discrepancies may reflect contribution of the intrinsic defect states. The calculated electron effective mass ratio (m_e^*/m_e) for $AgGaGe_2Se_6$ and $AgGaGe_5Se_{12}$ in the $\Gamma \rightarrow L$ direction is 0.0452 and 0.0397. We also have calculated the effective mass of the heavy holes and light holes.

AUTHOR INFORMATION

Corresponding Author

*Phone: +420 777 729 583. Fax: +420-386 361 219. E-mail: maalidph@yahoo.co.uk.

Notes

The authors declare no competing financial interest.

ACKNOWLEDGMENTS

The result was developed within the CENTEM project, reg. no. CZ.1.05/2.1.00/03.0088, cofunded by the ERDF as part of the Ministry of Education, Youth and Sports OP RDI programme. School of Material Engineering, Malaysia University of Perlis, Malaysia. S.A., would like to thank the CSIR-National Physical Laboratory for financial assistance.

REFERENCES

(1) Petrov, V.; Ghotbi, M.; Kokabee, O.; Esteban-Martin, A.; Noack, F.; Gaydardzhiev, A.; Nikolov, I.; Tzankov, P.; Buchvarov, I.; Miyata, K.; et al. Femtosecond Nonlinear Frequency Conversion Based on BiB_3O_6. *Laser Photonics Rev.* **2010**, *4*, 53−98.

(2) Wasylak, J.; Kucharski, J.; Golis, E.; Sahraoui, B.; Kityk, I. V. Photoinduced Phenomena in Sb_2Se_3-$BaCl_2$-$PbCl_2$ Glasses. *Proc. SPIE* **1999**, *3731*, 72−86.

(3) Badikov, V.; Mitin, K.; Noack, F.; Panyutin, V.; Petrov, V.; Seryogin, A.; Shevyrdyaeva, G. Orthorhombic Nonlinear Crystals of $Ag_xGa_xGe_{1-x}Se_2$ for the Mid-Infrared Spectral Range. *Opt. Mater.* **2009**, *31*, 590−597.

(4) Pobedimskaja, E. A. P.; Alimowa, L. I.; Belov, N. V.; Badikov, V. V. Crystalline Structure of Ag-sulphide and GeS_2. *Crystallography* **1980**, 611−614.

(5) Hughes, O. H.; Wolley, J. C.; Lopez-Rivera, S. A.; Pamplin, B. R. Quaternary Adamantine Selenides and Tellurides of the form I III IV VI_4. *Solid State Commun.* **1980**, *35*, 573−575.

(6) Badikov, V. V.; Tyulyupa, A. G.; Shevyrdyaeva, G. S.; Sheina, S. G. Solid Alloys in Systems $AgGaS_2$−GeS_2, $AgGaSe_2$−$GeSe_2$, Izv.AN SSR. *Inorg. Mater.* **1991**, *27*, 248−252.

(7) Olekseyuk, I. D.; Gulyak, A. V.; Sysa, L. V.; Gorgut, G. P.; Lomzin, A. F. Crystal Chemical Properties and Preparation of Single Crystals of $AgGaSe_2$−$GeSe_2$ γ-Solid Solutions. *J. Alloys Compd.* **1996**, *241* (1−2), 187−190.

(8) Fedorchuk, A. O.; Gorgut, G. P.; Parasyuk, O.; Lakshminarayana, G. V.; Kityk, I. V.; Piasecki, M. IR Operated Novel $Ag_{0.98}Cu_{0.02}GaGe_3Se_8$ Single Crystals. *J. Phys. Chem. Solids* **2011**, *72*, 1354−1357.

(9) Burak, Ya.V.; Dovgii, Ya.O.; Kityk, I. V. Optical Functions of $Li_2B_4O_7$ Crystals. *Opt. Spectrosc.* **1990**, *69* (N5), 702−708.

(10) Lemercier, G.; Andraud, C.; Kityk, I. V.; Ebothe, J.; Robertson, B. Birefringence in Guest−Host Ru-Containing Chromophore Induced by Acoustic Field. *Chem. Phys. Lett.* **2004**, *400*, 19−22.

(11) Grande, T.; Ishii, M.; Akaishi, M.; Aasland, S.; Fjellvag, H.; Stolen, S. Structural Properties of $GeSe_2$ at High Pressures. *J. Solid State Chem.* **1999**, *145*, 167−173.

(12) Blaha, P.; Schwarz, K.; Madsen, G. K. H.; Kvanicka, D.; Luitz, J. 2001 WIEN2K, An Augmented Plane Wave Plus Local Orbital Program for Calculating Crystal Properties, Karlheinz Schwarz; Techn. Universitat Wien: Austria. ISBN: 3-9501031-1-1-2.

(13) Ceperley, D. M.; Alder, B. I. Ground State of the Electron Gas by a Stochastic Method. *Phys. Rev. Lett.* **1980**, *45*, 566−569.

(14) Perdew, J. P.; Burke, K.; Ernzerhof, M. Generalized Gradient Approximation Made Simple. *Phys. Rev. Lett.* **1996**, *77*, 3865−3868.

(15) Engel, E.; Vosko, S. H. Exact Exchange-Only Potentials and the Virial Relation as Microscopic Criteria for Generalized Gradient Approximations. *Phys. Rev. B* **1993**, *47*, 13164−13174.

(16) Koller, D.; Tran, F.; Blaha, P. Merits and Limits of the Modified Becke-Johnson Exchange Potential. *Phys. Rev. B* **2011**, *83*, 195134−195143.
(17) Kityk, I. V.; Golis, E.; Filipecki, J.; Wasylak, J.; Zacharko, V. M. Photoinduced Nonlinear Optical Phenomena in PbO-$BiO_{1.5}$-$GaO_{1.5}$ Glass. *J. Mater. Sci. Lett.* **1995**, *14*, 1292−1293.
(18) Golis, E.; Kityk, I. V.; Wasylak, J.; Kasperczyk, J. Nonlinear Optical Properties of Lead-Bismuth-Gallium Glasses. *Mater. Res. Bull.* **1996**, *31*, 1057−1065.
(19) Kityk, I. V.; Zmija, J.; Majchrowski, A.; Ebothe, J. Acoustically Induced Optical Second Harmonic Generation in $Pb_{4.7}Ba_{0.3}Ge_3O_{11}$ Crystals. *J. Appl. Phys.* **2003**, *93*, 1160−1164.
(20) Dovgii, Ya. O.; Kityk, I. V. Band Structure and Nonlinear Optical Susceptibilities of Proustite (Ag_3AsS_3). *Phys. Status Solidi* **1991**, *166 B*, 395−402.
(21) Dovgii, Ya.O.; Kityk, I. V.; Man'kovskaya, I. G.; Evstigneeva, L. N. Polarized Light Spectrum of Tl_3SbS_3 Single Crystals. *Phys. Semicond.* **1990**, *24*, 1004−1005.
(22) Kityk, I. V.; Ebothe, J.; Ozga, K.; Plucinski, K. J.; Chang, G.; Kobayashi, K.; Oyama, M. Non-Linear Optical Properties of the Ag Nanoparticles on the ITO. *Physica E* **2005**, *31*, 38−42.
(23) Fasquelle, D.; Carru, J.-C.; Renard, C. Electrical characterizations of silver chalcogenide glasses. *J. Non-Cryst. Solids* **2007**, *353*, 1120−1125.
(24) Reshak, A. H.; Chen, X.; Auluck, S.; Kityk, I. V. X-ray Diffraction and Optical Properties of a Noncentrosymmetric Borate $CaBiGaB_2O_7$. *J. Chem. Phys.* **2008**, *129*, 204111−19.
(25) Delin, A.; Ravindran, P.; Eriksson, O.; Wills, J. M. Full-Potential Optical Calculations of Lead Chalcogenides. *Int. J. Quantum Chem.* **1998**, *69*, 349.
(26) Ching, W. T.; Rulis, P. Ab initio Calculation of the Electronic Structure and Spectroscopic Properties of Spinel γ-Sn3N4. *Phy. Rev. B* **2006**, *73*, 045202.
(27) Penn, D. R. Wave-Number-Dependent Dielectric Function of Semiconductors. *Phys. Rev.* **1962**, *128*, 2093−2097.
(28) Zhang, L.; Atuchin, V.; Kidyarov, B.; Andreev, Y. 2nd International Symposium on Laser Interaction with Matter (LIMIS 2012). *Proc. SPIE* **2013**, *8796*, 87962A.